A gain-of-function recurrent missense variant leads to a GABAergic/glutamatergic imbalance in a forebrain organoid model of PACS1 syndrome

Authors

Lauren E. Rylaarsdam,[1,2] Jennifer Rakotomamonjy,[1] Eleanor G. Pope,[1,3] Alicia Guemez-Gamboa[1*]

Affiliations

[1]Department of Neuroscience, Feinberg School of Medicine, Northwestern University, Chicago IL
[2]Interdepartmental Neuroscience graduate program, Northwestern University, Chicago, IL
[3]Undergraduate research program, Northwestern University, Chicago IL
*Correspondence: alicia.guemez@northwestern.edu

Abstract

PACS1 syndrome is a neurodevelopmental disorder characterized by intellectual disability and craniofacial abnormalities resulting from a *de novo* p.R203W variant in phosphofurin acidic cluster sorting protein 1 (PACS1). PACS1 is known to play roles in both the endosomal pathway and nucleus, but little is known about how this variant affects the developing nervous system and patients have few therapeutic options. Here, we used stem cell-derived dorsal forebrain organoids to show that PACS1$^{(+/R203W)}$ cells share convergent molecular features of autism spectrum disorder (ASD) through a gain-of-function mechanism. These features include an aberrant propensity towards GABAergic differentiation, increased inhibitory synaptic density, and impaired expression of an ASD-specific gene network enriched at synapses. This work is the first to investigate the impact of the p.R203W variant on developing neural tissue and suggests a therapy that either clears p.R203W PACS1 or targets convergent pathological mechanisms of ASD could be beneficial for patients.

Teaser

Authors use cerebral organoids to characterize mechanisms of PACS1 syndrome and find excitatory/inhibitory imbalances.

MAIN TEXT

Introduction

Neurodevelopmental disorders including autism spectrum disorder (ASD) and intellectual disability (ID) are highly prevalent in the population, both affecting 1-2% of individuals. Despite the pervasiveness of these disorders, few therapies exist due to a myriad of challenges including the genetic heterogeneity, historic inaccessibility of nervous tissue, and diagnosis usually occurring after the brain has developed. In certain instances, the genetic etiology of a neurodevelopmental disorder can be traced to a single gene, providing a more constrained genetic background to study these disorders and work towards therapy development. PACS1 syndrome – a neurodevelopmental disorder caused by a single recurrent missense variant – represents one such condition.

PACS1 syndrome (MIM615009) was first reported in 2012 when two patients in an ID cohort were noted to have strikingly similar craniofacial abnormalities and comparable developmental delays. Upon sequencing, both individuals were found to have the same *de novo* c.607C>T variant in the gene encoding phosphofurin acidic cluster sorting protein 1 (PACS1), which results in an arginine to tryptophan (R203W) substitution. Expression of the variant in a zebrafish model also produced craniofacial abnormalities, supporting the hypothesis that this was the variant responsible for patient symptoms.(*1*) Over 200 patients have since been identified with the same p.R203W pathogenic variant along with one report of a patient with an R203Q

substitution.(*2–6*) All patients have ID and are also frequently afflicted with seizures, ASD, feeding dysfunction, and abnormal formation of other limbs and organs.(*3*)

Most previous research on PACS1 has focused on its endogenous function. From these studies, it is known the 963 amino acid-long protein contains four domains: an N-terminal atrophin-1 related region (ARR); the furin binding region (FBR), which binds to targets expressing a specific acidic cluster sorting motif;(*7*) a middle region with autoregulatory properties and a nuclear localization signal (NLS);(*8*) and a C-terminal region with unknown function. The FBR is where the PACS1 syndrome-causing variant is located, potentially interfering with its binding ability. These domains enable PACS1 to perform multifunctional roles in the endosomal pathway and nucleus. PACS1 was first discovered for its role in the endosomal pathway as a cytosolic sorting protein which binds to a phosphorylated acidic cluster motif and traffics targets to the *trans*-Golgi Network.(*8*, *9*) PACS1 was initially reported in the context of the endoprotease furin, but has since been shown to bind to dozens of other targets with roles in vesicle trafficking, ion transport, gene expression, and other processes.(*10–19*) Additionally, PACS1 has shuttling functions between the nucleus and the cytoplasm.(*20*) Roles of PACS1 in the nucleus – where it accumulates during the S phase of the cell cycle – include mediating DNA replication repair,(*21*, *22*) exporting of viral transcripts,(*23*) RNA binding,(*20*) and regulation of chromatin stability through interaction with histone deacetylase (HDAC) proteins.(*21*)

PACS1 is highly expressed in the brain during embryonic development and maintained at lower levels after birth, suggesting it plays an important role during neurodevelopment and continues to perform functions in adult tissues. Genome-wide association studies (GWAS) also suggest a broader role in neural development and function for *PACS1* as it has been identified as a susceptibility gene in severe early-onset obesity,(*24*) developmental delay,(*25*) and bipolar disorder.(*26*) However, the majority of research on PACS1's function in neurons has been in the context of Alzheimer's disease, where it has been shown to impact symptom onset by facilitating localization of the β-secretase BACE1 and the Vps10 sorting receptor homolog SORLA to the *trans*-Golgi Network.(*27*, *28*) The role of PACS1 during human neurodevelopment and the impact of the p.R203W variant have never been investigated, and very few therapeutic options exist for patients.(*29*)

In this study, we used induced pluripotent stem cell (iPSC)-derived forebrain organoids to begin to understand the impact of the PACS1 syndrome-causing variant in cortical development. We found the p.R203W variant acts in a gain-of-function manner (GOF) to produce disease phenotypes with strong overlap to convergent features of ASD. This includes ectopic GABAergic expression driven by known autism risk genes, an excitatory/inhibitory synaptic imbalance, and an upregulated gene network reported in many studies of ASD. Altogether these results revealed a striking similarity to previously proposed convergent pathologies of ASD – despite PACS1 syndrome being primarily associated with ID – highlighting the overlap between etiologies of the two disorders. This is the first study to investigate the impact of the PACS1 variant on a knock-in model of the developing brain and suggests that therapies which clear the variant-containing PACS1 protein or target convergent mechanisms of ASD could benefit PACS1 syndrome patients.

Results

PACS1 p.R203W variant does not impact cytoarchitectural organization of cerebral organoids

To investigate how the p.R203W variant in PACS1 impacts developing neural cell types, we generated dorsal forebrain organoids from control and two patient lines **(Fig. 1***A***)**. In addition, we introduced the heterozygous variant which leads to p.R203W into one control line and corrected it in the patient lines using CRISPR/Cas9 gene editing technology (**Fig. 1***A*; **Fig. S1***A-C*). PACS1$^{(+/+)}$ and PACS1$^{(+/R203W)}$ iPSCs were then directed towards excitatory dorsal forebrain neural cell types through exposure to an established sequence of growth factors (**Fig. S2***A*).(*30*, *31*) After 40 days of differentiation, organoids of both genotypes strongly expressed dorsal forebrain markers such as FOXG1, EMX1, and PAX6 (**Fig. 1***B-D;* **Fig. S2***B-F*). As previously shown in the literature, organoids spontaneously developed ventricular zone (VZ)-like

PAX6+SOX2+ rosette structures surrounded by an intermediate zone containing CTIP2+ and TBR1+ excitatory neurons (**Fig. S2***B-F*). No differences in the proportion of cells expressing progenitor and postmitotic neuron markers were found at day 40 (**Fig. S2***C*), suggesting a similar differentiation rate at this timepoint.

Since forebrain organoids are composed of heterogeneous cell types and very little was understood about the disorder, we performed single-cell RNA sequencing (scRNAseq) to globally investigate cell type-specific transcriptomic changes in PACS1$^{(+/R203W)}$ developing neural cells (see methods and **Fig. S3***A-C*). ScRNAseq at day 40 revealed six distinct cell groups in both genotypes including early and late radial glia, intermediate progenitors, newborn neurons, excitatory neurons, and a small group of vascular leptomeningeal cells (**Fig. 1***E*; **Fig. S3***D,E*; **Fig. S4***A*). Feature plots show distinct segregation from proliferative to mature neuron markers while *PACS1* is expressed broadly across cell groups (**Fig. 1***F*). In support of immunohistochemistry data, transcriptomic analysis also showed no differences in the proportions of cell types between PACS1$^{(+/R203W)}$ and control organoids, indicating they are developing similarly on a gross cytoarchitectural level (**Fig. 1***G***; Fig. S4***B-C*).

PACS1 p.R203W variant results in upregulation of risk genes for other neurodevelopmental disorders by a gain-of-function mechanism

To uncover molecular pathways dysregulated by the PACS1 p.R203W variant in distinct developing neural cell types, we performed differential gene expression analysis of forebrain organoid transcriptomes. Our conservative approach yielded a total of 637 combined unique differentially expressed genes (DEGs; **Table S1**) that we validated by also running DEG analysis against publicly available controls. These controls were generated with the same protocol, collected with the same timepoint, and had a strong correlation to samples used in this study (**Fig. S5-6**). Top DEGs from this approach (read more in methods; **Fig. S7***A*) were broadly expressed across cell types (**Fig. S7***B*) and included genes with known involvement in neuronal differentiation such as *ZIC1, ZIC2,* and *LHX9* in the newborn group and *DLX1* and *ARX* in the excitatory neuron group (**Fig. 2***A*). DEGs in the mature neuron group were strongly enriched for risk genes of NDDs with overlapping phenotypes to PACS1 syndrome including ID, epilepsy, cerebellar hypoplasia, and ASD (**Fig. 2***B*). This could suggest neurons are more severely affected in PACS1 syndrome than proliferative cell types.

To investigate if the observed DEGs in PACS1$^{(+/R203W)}$ cells were the result of PACS1 loss-of-function (LOF) or GOF – information critical for therapy development – we generated PACS1$^{(-/-)}$ iPSC lines by introducing a frameshift variant in exon 4 (**Fig. S1***B-E*) and differentiating them to forebrain organoids. PACS1$^{(-/-)}$ organoids also spontaneously developed VZ-like structures surrounded by postmitotic neurons and expressed expected markers of the dorsal forebrain (**Fig. S2***B-F*).

With this model, we next asked if the observed DEGs identified in PACS1$^{(+/R203W)}$ organoids were also mis-regulated in the PACS1$^{(-/-)}$ lines. We searched for candidates for validation that met three criteria: they were differentially expressed across pseudobulk to eliminate the need for a specific double-stain marker; a difference in expression between genotypes was visually evident in a feature plot; and the protein had a nuclear localization to increase the accuracy of immunohistochemistry quantifications. Of three top candidates shown in **Fig. 2***C* ZIC1, a zinc finger protein with known roles in neuronal differentiation, was chosen for validation because it is also an OMIM risk gene for PACS1 comorbidities ASD, ID, and cerebellar hypoplasia. Immunohistochemistry analysis was performed by comparing the ratio of ZIC1+ nuclei to CTIP2+ nuclei as an internal positive control due to variable penetrance of nuclear-targeting antibodies in organoid tissue. This technique confirmed upregulation of the ZIC1 protein in PACS1$^{(+/R203W)}$ organoids and showed PACS1$^{(-/-)}$ samples had the same levels as controls, suggesting the R203W variant operates under a GOF mechanism (**Fig. 2***D,E*).

Neurons in PACS1$^{(+/R203W)}$ organoids have a propensity towards GABAergic differentiation

To obtain a more comprehensive understanding of what pathways are affected in PACS1$^{(+/R203W)}$ cells, we

performed gene ontology (GO) analysis of DEGs in each cell type. Downregulated genes in PACS1$^{(+/R203W)}$ organoids were not enriched for specific processes. However, GO analysis of upregulated transcripts in PACS1$^{(+/R203W)}$ showed strong patterns: while the newborn neuron group had differentially expressed transcripts related to neuron migration and neurite outgrowth (**Fig S9***A,B*), the most mature neuron group showed enrichment for terms related to GABAergic differentiation, even though we utilized a directed dorsal forebrain organoid protocol (**Fig. 3***A*). The presence of a few GABAergic cells arising from dorsal forebrain lineages is not unexpected,(*32*) but they were much more prevalent in PACS1$^{(+/R203W)}$ organoids. GABAergic-related GO terms were enriched due to upregulation of genes such as *ARX, DLX1, DLX2, DLX5, DLX6-AS1,* and *GAD1* in PACS1$^{(+/R203W)}$ neurons (**Fig. 3***B,C*; **Fig. S8***A-C*). To validate these findings, we quantified the number of cells expressing GAD67, the protein product of *GAD1,* in day 40 organoids. As suggested by the transcriptomic data, we found that PACS1$^{(+/R203W)}$ organoids had a higher number of GAD67+ cells when compared to control organoids. We did not observe this increased number of GABAergic cells in the PACS1$^{(-/-)}$ organoids, further supporting the hypothesis that the p.R203W variant has a GOF effect (**Fig. 3***D,E*; **Fig. S8***E*).

Pseudotime analysis reveals a gene module driving ectopic GABAergic fate in excitatory neurons from PACS1$^{(+/R203W)}$ organoids

In feature plots, all GABAergic markers segregated to the same branch of the neuron cluster (**Fig. 3***C*). The colocalization of GABAergic markers was intriguing as the collective transcriptome of this cluster correlated most highly to excitatory neurons in a reference dataset (*33*) (**Fig. S10**A) and expressed dorsal forebrain markers such as *CTIP2* and postmitotic *PAX6* (i.e. without colocalization of *MKI67*), but not classic ganglionic eminence markers such as *NKX2.1* or subpallial neuron marker *NR4A2* (**Fig. 4***A*, **Fig. S10***B*). These cells therefore had simultaneous GABAergic and glutamatergic properties and seemed unable to achieve proper specification.

We next asked what genes might be driving this fate decision towards an aberrant GABAergic-like trajectory in PACS1$^{(+/R203W)}$ organoids by employing pseudotime analysis.(*34*) Since an increase in GABAergic cells was not found in PACS1$^{(-/-)}$ organoids (**Fig. 3***D,E*), we did not include this genotype in subsequent investigations. Construction of the pseudotime trajectory with PACS1$^{(+/+)}$ and PACS1$^{(+/R203W)}$ cells showed a clear path from radial glia to neurons as pseudoage increased (**Fig. 4***B*). A single trajectory was generally followed until a divergence into hydra-like branches at the neuron cluster.

To look at which genes might be driving the fate decision of cells in the GABAergic-like branch, we first grouped genes that varied highly over pseudotime into modules of similar expression patterns. Then, we enhanced the granularity of the neuron group by increasing the cluster resolution parameter (**Fig. 4***C*) and plotted aggregate expression of each module in these subclusters (**Fig. 4***D*). This method allowed isolation of genes specifically expressed at the GABAergic fate point. Intriguingly, one module of 78 genes – arbitrarily numbered module 21 – was specifically and highly expressed just prior to the GABAergic fate point (boxed subclusters in **Fig. 4***D*) and was distinct from classically GABAergic genes in module 51 (**Table S3**). This gene set was enriched for transcripts known to play a role in suppression of excitatory or promotion of inhibitory differentiation, such as *ZIC1, ZIC2, MEF2C,* and *FOXG1.*(*35–38*) Module 21 was drastically more expressed in PACS1$^{(+/R203W)}$ organoids compared to controls (**Fig. 4***E,F*) and was in fact the most differentially expressed gene set between genotypes in cells just entering the GABAergic branch (**Fig. 4***G*). These results suggest that module 21 genes are involved in the fate decision of aberrant GABAergic specification in PACS1$^{(+/R203W)}$ neurons.

Neurons in PACS1$^{(+/R203W)}$ organoids have a higher density of GABAergic, but not glutamatergic synapses

In addition to promoting GABAergic and suppressing glutamatergic differentiation, module 21 genes such as *MEF2C* and *FOXG1* have previously been shown to regulate excitatory/inhibitory synaptic density.(*36*, *37*, *39*) Since this balance plays a critical role in disease mechanisms of neurodevelopmental disorders such as ASD and epilepsy,(*40*) we next investigated if excitatory/inhibitory balance might be impaired in PACS1

syndrome. As a proxy for number of synapses, we plotted collective expression of transcripts encoding glutamatergic or GABAergic receptors or transporters from our scRNAseq data, a complete list of which can be found in **Fig. S11***A.* The percentage of transcripts encoding glutamatergic synapse components was unaffected between genotypes (**Fig. 5***A*) but expression of GABAergic synaptic components was drastically upregulated (**Fig. 5***B*). We next looked at the relationship of glutamatergic and GABAergic receptor and transporter expression within the same cell. A small correlation was found in control neurons (**Fig. S11***B*), suggesting that neurons with more synapses – perhaps more mature cells – are the ones expressing GABAergic transcripts. In contrast, PACS1$^{(+/R203W)}$ neurons had no correlation between GABAergic and glutamatergic receptor and transporter expression (**Fig. S11***C*), suggesting a collective upregulation rather than an increase in a specific more inhibitory-like population.

To directly look at synapses on a protein level, we performed immunostaining in organoids. Since synapses are a very mature neuronal structure, we transitioned to day 80 organoids for validation. As shown in the literature, day 80 organoids of both genotypes demonstrated abundant expression of dorsal forebrain markers, transition of VZ-like structures to postmitotic identity, and emergence of mature neuron marker SATB2 (**Fig. S2***B,E,F*). To quantify synapses, we stained for a pre- and post-synaptic marker and quantified the colocalized puncta (**Fig. 5***C*). In support of the transcriptomic analysis, we observed an increase in the density of inhibitory but not excitatory synapses in PACS1$^{(+/R203W)}$ organoids (**Fig. 5***D*; **Fig. S11***D,E*), suggesting a further mechanism of excitatory/inhibitory (E/I) signaling imbalance in PACS1$^{(+/R203W)}$ organoids.

Gene co-expression analysis reveals an ASD-specific network upregulated in PACS1$^{(+/R203W)}$ neurons

Previous results such as ectopic GABAergic expression and an impaired E/I synaptic balance were remarkably similar to hypothesized convergent mechanisms of ASD. This is intriguing as PACS1 syndrome is caused by a single variant with best-known roles in the *trans*-Golgi Network and nucleus, while ASD is typically caused by a collective burden of many variants, often in synaptic genes. To further investigate the shared molecular signature of PACS1 syndrome and ASD, we employed weighted gene co-expression network analysis (WGCNA).(*41*) This powerful tool for analyzing RNA sequencing data enables identification of modules of genes with common expression patterns and has the ability to correlate them to external traits such as genotype. It is frequently used in studies of disorders with diverse etiologies to identify convergent mis-regulated gene networks.

We employed WGCNA on the transcriptome of equal numbers of PACS1$^{(+/R203W)}$ and control cells (**Fig. 6***A*). Ten distinct modules of gene expression were identified, five of which were significantly associated with genotype (**Fig. 6***B,C*). The arbitrarily named turquoise, brown, and blue modules (**Fig. 6***D*; **Table S3**) were selected for further investigation because these modules had a positive correlation between a gene's significance to the genotype and its interconnectedness within a module (**Fig. S12***A-C*). To determine if any gene modules correlated to those identified in other studies of autism, we extracted ASD neuronal-specific modules in eight landmark studies and performed a gene overlap test.(*37*, *42–48*) Intriguingly, we found that the "blue" module composed of 205 genes (**Table S3**) specifically and highly correlated with at least one module from all these studies (**Fig. 6***E*) as well as one convergent network identified in epilepsy context.(*49*) This module was unique to the excitatory neuron group – when the same analysis was performed in newborn neurons, a module correlating to the blue module in neurons was not identified, and there was no overlap with previously identified ASD-specific modules (**Fig. S12***D,E*).

To determine the functional significance of this blue module, we performed gene ontology analysis. Biological process analysis showed extremely strong enrichment for neurodevelopmental processes (**Fig. S12***F*) and module members with the most intra-modular connections – such as *GAP43, BASP1, STMN1,* and *UCHL1* – are well-known for their roles in neurodevelopment (**Fig. 6***D*). We next performed cellular component analysis and found enrichment for synaptic terms, suggesting that members of this upregulated module of genes were enriched for synaptic functions, a structure known to be specifically affected in ASD (**Fig. 6***F*). This suggests a previously uncharacterized role for either PACS1 or its binding partners at synapses and is an intriguing area of future investigation.

Discussion

Here we present some of the first work investigating the impact of the PACS1 p.R203W variant on the developing brain. A common thread through our results was the striking similarity to proposed convergent mechanisms of autism, such as aberrant GABAergic differentiation driven by ASD risk genes, an excitatory/inhibitory synaptic imbalance, and an upregulated network of genes found in other studies of ASD. Suppressed GABAergic inhibition was one of the first proposed convergent phenotypes of ASD in 2001 and continues to be a well-established hypothesis, particularly a hypofunction in parvalbumin-expressing interneurons.(*50–54*) However, other studies have also reported an increased density of GABAergic cells in ASD models, including a recent paper showing pathogenic mechanisms of *ARIDB*$^{+/-}$, *SUV420H1*$^{+/-}$, and *CHD8*$^{+/-}$ organoids converged toward early GABAergic induction.(*37*, *55–58*) Of course, certain discrepancies may arise from limitations in model systems in addition to genetic background, such as *in vitro* cultures lacking the circuitry and diversity of a functioning brain. The relative simplicity of an *in vitro* model is likely the reason for the apparent discrepancy between increased GABAergic cells in our PACS1$^{(+/R203W)}$ organoids and the epilepsy experienced by patients. While much more is left to understand, an accumulation of evidence suggests the excitation/inhibition balance is in some way impaired in the majority (if not all) of ASD cases.(*36*, *40*, *50–55*, *59–64*)

In this study, though we used an excitatory glutamatergic forebrain differentiation protocol, upregulation of GABAergic markers on the transcriptomic and protein level were found in PACS1$^{(+/R203W)}$ organoids. These cells co-expressed excitatory markers such as *CTIP2*, suggesting an aberrant co-occurrence of excitatory and inhibitory properties in PACS1$^{(+/R203W)}$ neurons. We used pseudotime analysis to show these GABAergic characteristics were driven by a module of known ASD risk genes including *MEF2C* and *FOXG1.* This is in line with previous reports showing a FOXG1-dependent GABAergic/glutamatergic imbalance in ASD organoid models (*37*) and MEF2C regulation of excitatory/inhibitory synaptic density.(*36*) This cluster also included many *ZIC* proteins, which have been shown to induce the generation of calretinin-positive GABAergic neurons (*35*) in addition to their more well-known roles in the cerebellar development. Intriguingly, a prevalent brain malformation in PACS1 patients is cerebellar hypoplasia, (*3*) which could have a mechanistic etiology in ZIC1.

Perhaps the strongest support for PACS1 syndrome's parallel to ASD was found with our co-expression network analysis, which identified an upregulated module of genes in PACS1$^{(+/R203W)}$ neurons that highly correlated to ASD-specific modules found in eight other high-profile studies. The degree of specificity was also notable as no other module – even those significantly associated with genotype – ever overlapped. No genes were present in every single one of these modules, but highly recurrent genes were strongly enriched for synapses. Members of the blue module itself were also enriched at synapses, which are considered a convergent affected structure in ASD and were found to have an impaired E/I ratio in this study.(*65*)

An additional key insight from this study is evidence for the PACS1 p.R203W variant operating in a GOF manner. ZIC1 and GAD67 were both increased in the PACS1$^{(+/R203W)}$ organoids, but PACS1$^{(-/-)}$ knockout organoids had the same levels as the controls. Our results implicate a GOF over a LOF since PACS1$^{(+/R203W)}$ and PACS1$^{(-/-)}$ organoids had different phenotypes. However, we do not yet know by what molecular mechanism the tryptophan substitution confers toxicity. Future studies should involve crystallography to try and resolve the structure of the FBR in the mutant and control PACS1, immunoprecipitation assays in neurons to establish if binding partners are lost or acquired upon introduction of the variant, binding affinity assays to determine if p.R203W binds variably to targets, and immunohistochemistry of PACS1 and its targets to assess how the variant impacts localization in the cell.

The GOF hypothesis supported by this study is reinforced in previous literature. The only study to date that directly looked at p.R203W PACS1 showed zebrafish exhibited craniofacial deficits when overexpressing p.R203W – but not wild-type – PACS1 mRNA.(*1*) The presence of endogenous PACS1 in this study suggests a GOF effect. Evidence against a LOF mechanism is further supported by a report of a family with a multi-exon deletion in PACS1 having little to no cognitive impairment, craniofacial abnormalities, or structural brain abnormalities.(*66*) Moreover, Pacs1$^{(-/-)}$ mice present with a deficiency of circulating B cells,

$CD4^+$ T cells, and $CD8^+$ T cells, but an absence of gross neurological phenotypes.(*67*) These findings implicate that an effective therapy for PACS1 syndrome patients could be clearing of the variant-containing protein. One potential approach to achieve this is with anti-sense oligonucleotides (ASOs) designed to bind in a complementary manner to the variant-containing mRNA and block translation. More studies should be done to determine if clearing p.R203W PACS1 with ASOs would be a safe and effective treatment.

Therapies such as ASOs provide much promise for PACS1 patients. Unfortunately, most other genetic causes of ASD and ID are much more complex and developing therapies for each genetic origin is very challenging. A momentous leap forward for the field would be to develop a way to target common phenotypes across a multitude of etiologies, such as restoring the excitation/inhibition balance. This is a monumental task, but the potential provides hope for PACS1 patients and millions of others suffering from ID and ASD.

Materials and Methods

Culture of iPSCs

Induced pluripotent stem cells were maintained in mTeSR+ medium (Stem Cell Technologies, 05825) on plates pre-coated with Matrigel (Corning, 354234) dissolved in DMEM/F12 at a concentration of 10 µg/mL. Stem cells were passaged as needed using ReLeSR medium (Stem Cell Technologies, 05872). Two control lines GM03651 and GM03652 were purchased from Coriell. A second control line S033751*B/GM27160 and two patient lines, S033745*B/GM27159 and PACS1003i-GM27161, were purchased from WiCell. An isogenic counterpart of each of these lines (except GM27160 and GM03652) was generated using CRISPR/Cas9. All cell lines were regularly tested for mycoplasma contamination and genotyped with Sanger sequencing.

CRISPR gene editing

Generation of isogenic cell lines was carried out utilizing the CRISPR/Cas9 system. Briefly, the Cas9 was delivered to cells as a px459-derived plasmid (Addgene, 62988) with a cloned guide that was designed using crispr.mit.edu software. The forward sequence was: caccgTTACAAGAATCGGACCATCT and reverse: aaacAGATGGTCCGATTCTTGTAAc (lowercase letters are sticky ends to clone into the plasmid). 5 µg of plasmid and 5 µg of donor DNA (sequence TGCAGATCATGCTGCAAAGGAGAAAACGTTACAAGAAT**T**GGACTATCTTAGGCTATAAGACCT TGGCCGTGGGACTCATCAAC) were delivered to 1 million cells using the NEON transfection system (ThermoFisher, MPK5000). 24 hours after electroporation, cells were exposed to 0.5 µg/mL puromycin for 24 hours to select for cells without the plasmid. Cells were left to expand for roughly 10 days. When visible colonies had formed, they were manually isolated with a pipet and Sanger sequenced. DNA from clones of interest was sent to Novogene for whole genome or whole exome sequencing. Analysis of top off-target sites predicted with CHOPCHOP and Benchling did not reveal any unintended edits.

Generation of forebrain organoids

Forebrain organoids were generated according to the previously described protocol by Sloan and coworkers, with slight modifications.(*31*) In brief, iPSCs were grown on matrigel-coated plates in mTeSR medium until colonies were ~ 5 mm across. Colonies were detached from the plate by incubating at 37ºC with 0.35 mg/mL dispase for 20 minutes. Detached colonies were then transferred to an ultra-low attachment dish (Corning, cat. no. 3262) with DMEM/F12 (1:1, Life Technologies, 1130-032) containing 20% vol/vol knockout serum replacement (Life Technologies, cat. no. 10828-028), 1% vol/vol non-essential amino acids (Life Technologies, 1140-050), 0.1 mM 2-mercaptoethanol (Sigma-Aldrich, M3148), 5 µM of the SMAD inhibitor dorsomorphin (Sigma-Aldrich, P5499), 10 µM SMAD inhibitor SB-4321542 (R&D Systems/Tocris, cat. no. 1614), and 10 µM rock inhibitor Y-27632 (Selleckchem, S1049). Media was changed daily for the next five days with the same reagents as described above, minus the Y-27632. At day 6, media was changed to a Neurobasal-A base containing 1x B-27, 1x Glutamax, 20 ng/mL FGF2, and 20

ng/mL EGF (R&D Systems, 236-EG). This media was changed every other day until day 25. At day 25, growth factors were switched to 20 ng/mL BDNF (PeproTech 450-02) and 20 ng/mL Neurotrophin 3 (PeproTech, cat. no. 450-03). Organoids were transitioned to neurobasal-A medium supplemented with 1x B-27 beginning at day 43 and continuing until the desired endpoint.

Dissociation of forebrain organoids for scRNAseq

Dissociation was done using the Worthington Papain Dissociation System (LK003150). Steps were done with sterile materials in a tissue culture hood. At day 40-42, two organoids between 3-4mm were selected per genotype. Organoids were pooled and washed with PBS + 0.2% BSA, then chopped into ~0.5mm pieces using a #10 blade. Organoids were incubated in a sterile-filtered 5 mL solution containing 20 U/mL papain in 1x EBSS, 0.46% sucrose, 26mM NaHCO3 (included in kit), 0.5mM EDTA (included in kit), and DNase (included in kit) equilibrated with 95%O2:5%CO2. Organoid pieces were incubated for 75 minutes on a 95 RPM orbital shaker in a 37ºC incubator. Following incubation, organoids were triturated using wide bore tips (Rainin, 30389218) and transferred to a 15 mL conical vial. Cells were spun 300xg for 5 minutes. The pellet was resuspended in a 3 mL papain inhibitor solution containing 2 mg/mL ovomucoid inhibitor, 2 mg/mL albumin, 0.46% sucrose, and DNase in 1x EBSS (all from Worthington kit LK003150). This cell suspension was gently applied on top of a 5 mL solution of 10 mg/mL ovomucoid inhibitor, 10 mg/mL albumin, and 0.46% sucrose to create a density gradient. The gradient was spun at 70xg for 6 minutes. The pellet was washed with 5 mL PBS + 0.2% BSA and spun again at 300xg for 5 minutes. The pellet was resuspended in 130 µL PBS + 0.2% BSA and filtered to remove cell clumps (Bel-Art, H13680-0040), resulting in the final single-cell suspension. In total, seven samples were processed in three distinct batches (pictured in **Fig. S3***A*).

ScRNAseq analysis

Preparation of samples was carried out as described above. Samples were only processed if viability of the dissociation was >85%. The library prep was conducted by Northwestern's Center for Genetic Medicine using the 10x Chromium library prep system. Sequencing was done using 100bp, paired-end reads on an Illumina HiSeq 4000 with one sequencing lane per sample. Raw data was demultiplexed and FASTQ files were processed using the CellRanger pipeline.

After sequencing, we analyzed the data using Seurat and Monocle3 packages in R.(*34*, *68*, *69*) In Seurat, data was filtered for nFeature_RNA > 500, nFeature_RNA < 6500, and percent mitochondrial reads < 15. For each sample, doublets were first identified by performing processing steps (NormalizeData, FindVariableFeatures, ScaleData, RunPCA, FindNeighbors, FindClusters, RunTSNE) and then running two separate doublet finding packages: DoubletFinder and DoubletDecon.(*70*, *71*) Barcodes were extracted for consensus cells that both packages identified as doublets (roughly 5% of each sample). Following doublet identification (a schematic is shown in **Fig. S3***B*), analysis was re-started, and doublets were removed in the initial filtering steps. Samples were merged and then NormalizeData and FindVariableFeatures were performed on each sample. A FindIntegrationAnchors step was done to enable comparative visualization across samples, followed by IntegrateData. After integration, the ScaleData, RunPCA, FindNeighbors, FindClusters, and RunTSNE steps were performed. For differential expression analysis, public data (GSM3885398, GSM3885387, ERS4649261, ERS4649262, and ERS4649263) was incorporated by projecting onto pre-existing data using the TransferAnchors step. Cluster identification was bioinformatically aided with the Clustifyr package (*72*) using a fetal human tissue dataset generated in the Kriegstein lab as a reference.(*33*) Cluster names were simplified to represent the broad cell type classification.

Differential expression analysis was performed using the FindMarkers function. To increase the power for this analysis, five additional public controls (GSM3885398, GSM3885387, ERS4649261, ERS4649262, and ERS4649263) generated with the same differentiation protocol and nearly identical timepoint were downloaded from the NCBI GEO repository.(*73*, *74*) The relationship between samples in this study and public controls is explored in **Fig. S5-6**. To reduce the number of false positives caused by inter-organoid

variability, FindMarkers was performed six ways: between three different groups of controls (organoids generated in the Guemez-Gamboa lab, Kriegstein lab, and Testa labs) and two different batches of PACS1$^{(+/R203W)}$ organoids. Only hits up or downregulated in all five+ tests with an average adjusted *p* value of < 0.05 after Bonferroni correction for all genes were included as DEGs (**Fig. S7*A*; Table S1)**. "Top" DEGs were significant for all six tests. Mitochondrial (MT-) and ribosomal (RPS/RPL) proteins were removed for GO and DAVID analysis.

Pseudotime analysis

Pseudotime analysis was performed by closely following tutorials developed by Cole Trapnell at cole-trapnell-lab.github.io/monocle3/ and integrated with Seurat using the SeuratWrappers function. First, a cell data set object was created from the fully processed Seurat object containing all seven samples. Cluster_cells, preprocess_cds, estimate_size_factors, and learn_graph functions were used to generate a pseudotime trajectory graph. The root node was manually chosen and only the largest partition was used, which contained all the neurons. Graph_test, find_gene_modules, and aggregate_gene_expression functions were used to group modules of gene expression over pseudotime. Downstream analysis was performed with base Seurat and Monocle3 functions.

WGCNA

To perform weighted co-expression network analysis, 4,884 control and PACS1$^{(+/R203W)}$ neurons were randomly subsetted from the Seurat object. Data was processed closely following tutorials developed by Peter Langelder and Steve Horvath from horvath.genetics.ucla.edu. First, a data frame of each cell's expression of all genes was made. Genes and samples with too many missing values were removed with the function goodSamplesGenes. The blockwiseModules function was run using a scale free topology power of 3, a signed TOM type, minimum module size of 30, and a max block size of 50,000 so genes were not divided in blocks. This resulted in 10 distinct modules, 5 of which were significantly correlated with genotype. The abs and intramodularConnectivity functions were used to determine which modules had a positive correlation between a gene's interconnectedness within a module and significance to genotype. To test if modules overlapped with previously identified ASD modules, the geneOverlap package was used and *p* values were adjusted using a Benjamini-Hochberg correction.

Cryopreservation and sectioning

Organoids were fixed with 4% paraformaldehyde in PBS at 4ºC overnight. They were then washed with PBS and transferred to a 30% sucrose solution in PBS and incubated at 4ºC for at least 16 hours. To cryopreserve, organoids were embedded in OCT medium using a mold and snap frozen in dry ice and ethanol. Organoids were stored at -80ºC indefinitely. Frozen organoids were sectioned 15-20 µm thick at -16ºC in a cryostat and applied to Thermofisher slides. Slides were left to dry overnight and then stored at -80ºC.

Immunohistochemistry

Organoid sections were dried for at least one hour either at room temperature or 37ºC. OCT was removed in a series of 3x10 min washes in PBS. An antigen retrieval step was performed by steaming slices at 99ºC for 10 minutes in a 10 mM citrate solution at pH 6.0. To remove the citrate buffer, slides were washed 1x5 min in dH_20 and 2x5 min in PBS. Tissue was blocked in a 10% NDS, 3% Triton X-100 solution in 1x PBS for 1-2 hours at room temperature. Following blocking, tissue was incubated in a 5% NDS, 1.5% Triton X-100 solution in 1x PBS containing primary antibodies at 4ºC overnight. Primary antibodies used in this study are: CTIP2 Abcam ab18465; PAX6 BioLegend 901301; TBR1 Proteintech 66564-1-Ig; SOX2 EMD Millipore AB5603; SATB2 Synaptic Systems 327004; FOXG1 Abcam ab196868; EMX1 Atlas Antibodies HPA006421; ZIC1 Invitrogen PA5-47681, GAD67 EMD Millipore MAB5406; SYN1 Cell Signaling Technology 5297; PSD95 NeuroMab K28/43; vGAT ThermoFisher PA5-27569; Gephyrin Synaptic Systems 147-021; TRA1-60 Sigma MAB4360; and OCT4A Cell Signaling Technology C30A3. The

overnight incubation was followed by 3x10 min PBS wash, then Alexa Fluor secondary antibody incubation at 1:200 in a 5% NDS, 1.5% Triton X-100 solution in 1x PBS for 90 minutes at room temperature. Excess antibodies were removed with 3x10 minute PBS washes and a 20-minute incubation in 2 µg/mL DAPI. Slides mounted with Fluoromount medium and imaged on a Nikon W1 spinning disk confocal microscope or BZX710 Keyence epifluorescent microscope. Images were analyzed using ImageJ (Fiji). All signal adjustments in Fiji were linear except a minor gamma adjustment in Fig. 1*B* for the EMX1 PACS1$^{(+/+)}$ stain. The linear adjustment version is in Fig. S2*F*.

Synaptic quantifications

Day 79 organoid sections were stained for MAP2 and either SYN1/PSD95 or vGAT/GPHN primary antibodies as described in the above section. Confocal images were taken on a Nikon W1 Dual CAM Spinning Disk microscope at 60x resolution with a 1 µm step size with a Z stack of 15 images, then collapsed to one plane in ImageJ based on maximal intensity. Pre- and post- synaptic puncta channels were converted to binary and superimposed, then the number of colocalizations above 10 pixels in area was automatically counted using the Analyze Particles macro.

Protein extraction and Western blotting

Proteins were extracted from 40-day-old neural organoids using RIPA buffer (9806, Cell Signaling Technology) supplemented with protease and phosphatase inhibitor cocktail (78440, Thermo Scientific). Protein concentration was determined using the Pierce BCA protein assay kit (23227, Thermo Scientific), and lysates were denatured by adding Laemmli buffer (1610747, Bio-Rad) and boiling at 95°C. 30 µg of protein extract was resolved on 4-15% polyacrylamide gels (4561085, Bio-Rad), transferred to PVDF membranes (88518, Thermo Scientific) and then immunoblotted with specific antibodies: anti-PACS1 (dilution 1:500, HPA038914, Sigma-Aldrich) and α-Tubulin (dilution 1:10,000, ab7291, Abcam). Membranes were then incubated with relevant near-infrared dyes-conjugated secondary antibodies (1:10,000, Li-Cor). Protein signal was detected using the Odyssey® Fc Imaging System (Li-Cor) and quantified with Image Studio (Li-Cor).

Statistical Analysis

All statistics for single-cell RNA sequencing data were performed in R while statistics for immunohistochemistry analysis was performed in Microsoft Excel. Detailed information on tests used for each experiment are in the figure legends.

References

1. J. H. M. Schuurs-Hoeijmakers, E. C. Oh, L. E. L. M. Vissers, M. E. M. Swinkels, C. Gilissen, M. A. Willemsen, M. Holvoet, M. Steehouwer, J. A. Veltman, B. B. A. de Vries, H. van Bokhoven, A. P. M. de Brouwer, N. Katsanis, K. Devriendt, H. G. Brunner, Recurrent *De Novo* Mutations in PACS1 Cause Defective Cranial-Neural-Crest Migration and Define a Recognizable Intellectual-Disability Syndrome. *Am. J. Hum. Genet.* **91**, 1122–1127 (2012).
2. D. Gadzicki, D. Döcker, M. Schubach, M. Menzel, B. Schmorl, F. Stellmer, S. Biskup, D. Bartholdi, Expanding the phenotype of a recurrent *de novo* variant in PACS1 causing intellectual disability. *Clin. Genet.* **88**, 300–302 (2015).
3. J. H. M. Schuurs-Hoeijmakers, M. L. Landsverk, N. Foulds, M. K. Kukolich, R. H. Gavrilova, S. Greville-Heygate, A. Hanson-Kahn, J. A. Bernstein, J. Glass, D. Chitayat, T. A. Burrow, A. Husami, K. Collins, K. Wusik, N. van der Aa, F. Kooy, K. T. Brown, D. Gadzicki, U. Kini, S. Alvarez, A. Fernández-Jaén, F. McGehee, K. Selby, M. Tarailo-Graovac, M. Van Allen, C. D. M. van Karnebeek, D. J. Stavropoulos, C. R. Marshall, D. Merico, A. Gregor, C. Zweier, R. J. Hopkin, Y. W.-Y. Chu, B. H.-Y. Chung, B. B. A. de Vries, K. Devriendt, M. E. Hurles, H. G. Brunner, DDD study, Clinical delineation of the PACS1-related syndrome--Report on 19 patients. *Am. J. Med. Genet. A.* **170**, 670–675 (2016).
4. A. Martinez-Monseny, M. Bolasell, C. Arjona, L. Martorell, D. Yubero, J. Arsmtrong, J. Maynou, G. Fernandez, M. del Carmen Salgado, F. Palau, M. Serrano, Mutation of PACS1: the milder end of the spectrum. *Clin. Dysmorphol.* **Publish Ahead of Print** (2018), doi:10.1097/MCD.0000000000000237.
5. D. Stern, M. T. Cho, R. Chikarmane, R. Willaert, K. Retterer, F. Kendall, M. Deardorff, S. Hopkins, E. Bedoukian, A. Slavotinek, S. S. Vergano, B. Spangler, M. McDonald, A. McConkie-Rosell, B. K. Burton, K. H. Kim, N. Oundjian, D.

Kronn, N. Chandy, B. Baskin, M. J. G. Sacoto, I. M. Wentzensen, H. M. McLaughlin, D. McKnight, W. K. Chung, Association of the missense variant p.Arg203Trp in PACS1 as a cause of intellectual disability and seizures. *Clin. Genet.* **92**, 221–223 (2017).
6. N. Miyake, S. Ozasa, H. Mabe, S. Kimura, M. Shiina, E. Imagawa, S. Miyatake, M. Nakashima, T. Mizuguchi, A. Takata, K. Ogata, N. Matsumoto, A novel missense mutation affecting the same amino acid as the recurrent PACS1 mutation in Schuurs-Hoeijmakers syndrome. *Clin. Genet.* **93**, 929–930 (2018).
7. G. Thomas, J. E. Aslan, L. Thomas, P. Shinde, U. Shinde, T. Simmen, Caught in the act - protein adaptation and the expanding roles of the PACS proteins in tissue homeostasis and disease. *J. Cell Sci.* **130**, 1865–1876 (2017).
8. G. K. Scott, F. Gu, C. M. Crump, L. Thomas, L. Wan, Y. Xiang, G. Thomas, The phosphorylation state of an autoregulatory domain controls PACS-1-directed protein traffic. *EMBO J.* **22**, 6234–6244 (2003).
9. L. Wan, S. S. Molloy, L. Thomas, G. Liu, Y. Xiang, S. L. Rybak, G. Thomas, PACS-1 Defines a Novel Gene Family of Cytosolic Sorting Proteins Required for trans-Golgi Network Localization. *Cell*. **94**, 205–216 (1998).
10. I. Hinners, F. Wendler, H. Fei, L. Thomas, G. Thomas, S. A. Tooze, AP-1 recruitment to VAMP4 is modulated by phosphorylation-dependent binding of PACS-1. *EMBO Rep.* **4**, 1182–1189 (2003).
11. M. Köttgen, T. Benzing, T. Simmen, R. Tauber, B. Buchholz, S. Feliciangeli, T. B. Huber, B. Schermer, A. Kramer-Zucker, K. Höpker, K. C. Simmen, C. C. Tschucke, R. Sandford, E. Kim, G. Thomas, G. Walz, Trafficking of TRPP2 by PACS proteins represents a novel mechanism of ion channel regulation. *EMBO J.* **24**, 705–716 (2005).
12. P. M. Jenkins, L. Zhang, G. Thomas, J. R. Martens, PACS-1 Mediates Phosphorylation-Dependent Ciliary Trafficking of the CNG Channel in Olfactory Sensory Neurons. *J. Neurosci. Off. J. Soc. Neurosci.* **29**, 10541–10551 (2009).
13. S. Taya, T. Shinoda, D. Tsuboi, J. Asaki, K. Nagai, T. Hikita, S. Kuroda, K. Kuroda, M. Shimizu, S. Hirotsune, A. Iwamatsu, K. Kaibuchi, DISC1 Regulates the Transport of the NUDEL/LIS1/14-3-3ε Complex through Kinesin-1. *J. Neurosci.* **27**, 15–26 (2007).
14. G. Gorini, O. Ponomareva, K. S. Shores, M. D. Person, R. A. Harris, R. D. Mayfield, Dynamin-1 co-associates with native mouse brain BKCa channels: proteomics analysis of synaptic protein complexes. *FEBS Lett.* **584**, 845–851 (2010).
15. K. B. Emdal, A.-K. Pedersen, D. B. Bekker-Jensen, K. P. Tsafou, H. Horn, S. Lindner, J. H. Schulte, A. Eggert, L. J. Jensen, C. Francavilla, J. V. Olsen, Temporal proteomics of NGF-TrkA signaling identifies an inhibitory role for the E3 ligase Cbl-b in neuroblastoma cell differentiation. *Sci. Signal.* **8**, ra40–ra40 (2015).
16. G. Giurato, G. Nassa, A. Salvati, E. Alexandrova, F. Rizzo, T. A. Nyman, A. Weisz, R. Tarallo, Quantitative mapping of RNA-mediated nuclear estrogen receptor β interactome in human breast cancer cells. *Sci. Data*. **5**, 180031 (2018).
17. Qiagen, Ingenuity Pathway Analysis.
18. M. N. Nenov, F. Laezza, S. J. Haidacher, Y. Zhao, R. G. Sadygov, J. M. Starkey, H. Spratt, B. A. Luxon, K. T. Dineley, L. Denner, Cognitive enhancing treatment with a PPARγ agonist normalizes dentate granule cell presynaptic function in Tg2576 APP mice. *J. Neurosci. Off. J. Soc. Neurosci.* **34**, 1028–1036 (2014).
19. C. D. Farr, P. R. Gafken, A. D. Norbeck, C. E. Doneanu, M. D. Stapels, D. F. Barofsky, M. Minami, J. A. Saugstad, Proteomic analysis of native metabotropic glutamate receptor 5 protein complexes reveals novel molecular constituents. *J. Neurochem.* **91**, 438–450 (2004).
20. S. M. Trothen, R. X. Zang, A. Lurie, J. D. Dikeakos, PACS-1 contains distinct motifs for nuclear-cytoplasmic transport and interacts with the RNA-binding protein PTBP1 in the nucleus and cytosol. *FEBS Lett.* **596**, 232–248 (2022).
21. C. Mani, K. Tripathi, S. Luan, D. W. Clark, J. F. Andrews, A. Vindigni, G. Thomas, K. Palle, The Multifunctional Protein PACS-1 is Required for HDAC2 and HDAC3 Dependent Chromatin Maturation and Genomic Stability. *Oncogene*. **39**, 2583–2596 (2020).
22. M. S. Veena, S. Raychaudhuri, S. K. Basak, N. Venkatesan, P. Kumar, R. Biswas, R. Chakrabarti, J. Lu, T. Su, M. Gallagher-Jones, M. Morselli, H. Fu, M. Pellegrini, T. Goldstein, M. I. Aladjem, M. B. Rettig, S. P. Wilczynski, D. S. Shin, E. S. Srivatsan, Dysregulation of hsa-miR-34a and hsa-miR-449a leads to overexpression of PACS-1 and loss of DNA damage response (DDR) in cervical cancer. *J. Biol. Chem.* **295**, 17169–17186 (2020).
23. H. Liu, P.-W. Hu, S. Budhiraja, A. Misra, J. Couturier, R. E. Lloyd, D. E. Lewis, J. T. Kimata, A. P. Rice, PACS1 is an HIV-1 cofactor that functions in Rev-mediated nuclear export of viral RNA. *Virology*. **540**, 88–96 (2020).
24. E. Wheeler, N. Huang, E. G. Bochukova, J. M. Keogh, S. Lindsay, S. Garg, E. Henning, H. Blackburn, R. J. F. Loos, N. J. Wareham, S. O'Rahilly, M. E. Hurles, I. Barroso, I. S. Farooqi, Genome-wide SNP and CNV analysis identifies common and low-frequency variants associated with severe early-onset obesity. *Nat. Genet.* **45**, 513–517 (2013).
25. Deciphering Developmental Disorders: Study, prevalence, and architecture of *de novo* mutations in developmental disorders. *Nature*. **542**, 433–438 (2017).
26. N. Mullins *et al.*, Genome-wide association study of more than 40,000 bipolar disorder cases provides new insights into the underlying biology. *Nat. Genet.* **53**, 817–829 (2021).
27. T. Burgert, V. Schmidt, S. Caglayan, F. Lin, A. Füchtbauer, E.-M. Füchtbauer, A. Nykjaer, A.-S. Carlo, T. E. Willnow, SORLA-Dependent and -Independent Functions for PACS1 in Control of Amyloidogenic Processes. *Mol. Cell. Biol.* **33**, 4308–4320 (2013).

28. V. Schmidt, A. Sporbert, M. Rohe, T. Reimer, A. Rehm, O. M. Andersen, T. E. Willnow, SorLA/LR11 Regulates Processing of Amyloid Precursor Protein via Interaction with Adaptors GGA and PACS-1. *J. Biol. Chem.* **282**, 32956–32964 (2007).
29. L. Rylaarsdam, T. Reddy, A. Guemez-Gamboa, In search of a cure: PACS1 Research Foundation as a model of rare disease therapy development. *Trends Genet.* **38**, 109–112 (2022).
30. F. Birey, J. Andersen, C. D. Makinson, S. Islam, W. Wei, N. Huber, H. C. Fan, K. R. C. Metzler, G. Panagiotakos, N. Thom, N. A. O'Rourke, L. M. Steinmetz, J. A. Bernstein, J. Hallmayer, J. R. Huguenard, S. P. Paşca, Assembly of functionally integrated human forebrain spheroids. *Nature*. **545**, 54–59 (2017).
31. S. A. Sloan, J. Andersen, A. M. Paşca, F. Birey, S. P. Paşca, Generation and assembly of human brain region–specific three-dimensional cultures. *Nat. Protoc.* **13**, 2062 (2018).
32. R. N. Delgado, D. E. Allen, M. G. Keefe, W. R. Mancia Leon, R. S. Ziffra, E. E. Crouch, A. Alvarez-Buylla, T. J. Nowakowski, Individual human cortical progenitors can produce excitatory and inhibitory neurons. *Nature*. **601**, 397–403 (2022).
33. T. J. Nowakowski, A. Bhaduri, A. A. Pollen, B. Alvarado, M. A. Mostajo-Radji, E. Di Lullo, M. Haeussler, C. Sandoval-Espinosa, S. J. Liu, D. Velmeshev, J. R. Ounadjela, J. Shuga, X. Wang, D. A. Lim, J. A. West, A. A. Leyrat, W. J. Kent, A. R. Kriegstein, Spatiotemporal gene expression trajectories reveal developmental hierarchies of the human cortex. *Science*. **358**, 1318–1323 (2017).
34. C. Trapnell, D. Cacchiarelli, J. Grimsby, P. Pokharel, S. Li, M. Morse, N. J. Lennon, K. J. Livak, T. S. Mikkelsen, J. L. Rinn, The dynamics and regulators of cell fate decisions are revealed by pseudotemporal ordering of single cells. *Nat. Biotechnol.* **32**, 381–386 (2014).
35. M.-C. Tiveron, C. Beclin, S. Murgan, S. Wild, A. Angelova, J. Marc, N. Coré, A. de Chevigny, E. Herrera, A. Bosio, V. Bertrand, H. Cremer, Zic-Proteins Are Repressors of Dopaminergic Forebrain Fate in Mice and C. elegans. *J. Neurosci. Off. J. Soc. Neurosci.* **37**, 10611–10623 (2017).
36. A. J. Harrington, A. Raissi, K. Rajkovich, S. Berto, J. Kumar, G. Molinaro, J. Raduazzo, Y. Guo, K. Loerwald, G. Konopka, K. M. Huber, C. W. Cowan, MEF2C regulates cortical inhibitory and excitatory synapses and behaviors relevant to neurodevelopmental disorders. *eLife*. **5**, e20059 (2016).
37. J. Mariani, G. Coppola, P. Zhang, A. Abyzov, L. Provini, L. Tomasini, M. Amenduni, A. Szekely, D. Palejev, M. Wilson, M. Gerstein, E. L. Grigorenko, K. Chawarska, K. A. Pelphrey, J. R. Howe, F. M. Vaccarino, FOXG1-Dependent Dysregulation of GABA/Glutamate Neuron Differentiation in Autism Spectrum Disorders. *Cell*. **162**, 375–390 (2015).
38. C. Mayer, C. Hafemeister, R. C. Bandler, R. Machold, R. Batista Brito, X. Jaglin, K. Allaway, A. Butler, G. Fishell, R. Satija, Developmental diversification of cortical inhibitory interneurons. *Nature*. **555**, 457–462 (2018).
39. R. A. Samarasinghe, O. A. Miranda, J. E. Buth, S. Mitchell, I. Ferando, M. Watanabe, T. F. Allison, A. Kurdian, N. N. Fotion, M. J. Gandal, P. Golshani, K. Plath, W. E. Lowry, J. M. Parent, I. Mody, B. G. Novitch, Identification of neural oscillations and epileptiform changes in human brain organoids. *Nat. Neurosci.* **24**, 1488–1500 (2021).
40. R. Gao, P. Penzes, Common Mechanisms of Excitatory and Inhibitory Imbalance in Schizophrenia and Autism Spectrum Disorders. *Curr. Mol. Med.* **15**, 146–167 (2015).
41. P. Langfelder, S. Horvath, WGCNA: an R package for weighted correlation network analysis. *BMC Bioinformatics*. **9**, 559 (2008).
42. M. J. Gandal, J. R. Haney, N. N. Parikshak, V. Leppa, G. Ramaswami, C. Hartl, A. J. Schork, V. Appadurai, A. Buil, T. M. Werge, C. Liu, K. P. White, CommonMind Consortium, PsychENCODE Consortium, iPSYCH-BROAD Working Group, S. Horvath, D. H. Geschwind, Shared molecular neuropathology across major psychiatric disorders parallels polygenic overlap. *Science*. **359**, 693–697 (2018).
43. S. Gupta, S. E. Ellis, F. N. Ashar, A. Moes, J. S. Bader, J. Zhan, A. B. West, D. E. Arking, Transcriptome analysis reveals dysregulation of innate immune response genes and neuronal activity-dependent genes in autism. *Nat. Commun.* **5**, 5748 (2014).
44. K. Griesi-Oliveira, M. S. Fogo, B. G. G. Pinto, A. Y. Alves, A. M. Suzuki, A. G. Morales, S. Ezquina, O. J. Sosa, G. J. Sutton, D. Y. Sunaga-Franze, A. P. Bueno, G. Seabra, L. Sardinha, S. S. Costa, C. Rosenberg, E. C. Zachi, A. L. Sertie, D. Martins-de-Souza, E. M. Reis, I. Voineagu, M. R. Passos-Bueno, Transcriptome of iPSC-derived neuronal cells reveals a module of co-expressed genes consistently associated with autism spectrum disorder. *Mol. Psychiatry*. **26**, 1589–1605 (2021).
45. I. Voineagu, X. Wang, P. Johnston, J. K. Lowe, Y. Tian, S. Horvath, J. Mill, R. M. Cantor, B. J. Blencowe, D. H. Geschwind, Transcriptomic analysis of autistic brain reveals convergent molecular pathology. *Nature*. **474**, 380–384 (2011).
46. N. N. Parikshak, V. Swarup, T. G. Belgard, M. Irimia, G. Ramaswami, M. J. Gandal, C. Hartl, V. Leppa, L. de la T. Ubieta, J. Huang, J. K. Lowe, B. J. Blencowe, S. Horvath, D. H. Geschwind, Genome-wide changes in lncRNA, splicing, and regional gene expression patterns in autism. *Nature*. **540**, 423–427 (2016).
47. S. T. Schafer, A. C. M. Paquola, S. Stern, D. Gosselin, M. Ku, M. Pena, T. J. M. Kuret, M. Liyanage, A. A. Mansour, B. N. Jaeger, M. C. Marchetto, C. K. Glass, J. Mertens, F. H. Gage, Pathological priming causes developmental gene network heterochronicity in autistic subject-derived neurons. *Nat. Neurosci.* **22**, 243–255 (2019).

48. E. Ben-David, S. Shifman, Networks of neuronal genes affected by common and rare variants in autism spectrum disorders. *PLoS Genet.* **8**, e1002556 (2012).
49. A. Delahaye-Duriez, P. Srivastava, K. Shkura, S. R. Langley, L. Laaniste, A. Moreno-Moral, B. Danis, M. Mazzuferi, P. Foerch, E. V. Gazina, K. Richards, S. Petrou, R. M. Kaminski, E. Petretto, M. R. Johnson, Rare and common epilepsies converge on a shared gene regulatory network providing opportunities for novel antiepileptic drug discovery. *Genome Biol.* **17**, 245 (2016).
50. J. P. Hussman, Suppressed GABAergic inhibition as a common factor in suspected etiologies of autism. *J. Autism Dev. Disord.* **31**, 247–248 (2001).
51. A. Contractor, I. M. Ethell, C. Portera-Cailliau, Cortical interneurons in autism. *Nat. Neurosci.* **24**, 1648–1659 (2021).
52. B. R. Ferguson, W.-J. Gao, PV Interneurons: Critical Regulators of E/I Balance for Prefrontal Cortex-Dependent Behavior and Psychiatric Disorders. *Front. Neural Circuits*. **12**, 37 (2018).
53. F. Filice, L. Janickova, T. Henzi, A. Bilella, B. Schwaller, The Parvalbumin Hypothesis of Autism Spectrum Disorder. *Front. Cell. Neurosci.* **14**, 577525 (2020).
54. H.-T. Chao, H. Chen, R. C. Samaco, M. Xue, M. Chahrour, J. Yoo, J. L. Neul, S. Gong, H.-C. Lu, N. Heintz, M. Ekker, J. L. R. Rubenstein, J. L. Noebels, C. Rosenmund, H. Y. Zoghbi, Dysfunction in GABA signalling mediates autism-like stereotypies and Rett syndrome phenotypes. *Nature*. **468**, 263–269 (2010).
55. B. Paulsen, S. Velasco, A. J. Kedaigle, M. Pigoni, G. Quadrato, A. J. Deo, X. Adiconis, A. Uzquiano, R. Sartore, S. M. Yang, S. K. Simmons, P. Symvoulidis, K. Kim, K. Tsafou, A. Podury, C. Abbate, A. Tucewicz, S. N. Smith, A. Albanese, L. Barrett, N. E. Sanjana, X. Shi, K. Chung, K. Lage, E. S. Boyden, A. Regev, J. Z. Levin, P. Arlotta, Autism genes converge on asynchronous development of shared neuron classes. *Nature* (2022), doi:10.1038/s41586-021-04358-6.
56. Y. A. Lawrence, T. L. Kemper, M. L. Bauman, G. J. Blatt, Parvalbumin-, calbindin-, and calretinin-immunoreactive hippocampal interneuron density in autism. *Acta Neurol. Scand.* **121**, 99–108 (2010).
57. P. Wang, R. Mokhtari, E. Pedrosa, M. Kirschenbaum, C. Bayrak, D. Zheng, H. M. Lachman, CRISPR/Cas9-mediated heterozygous knockout of the autism gene CHD8 and characterization of its transcriptional networks in cerebral organoids derived from iPS cells. *Mol. Autism*. **8**, 11 (2017).
58. M. C. N. Marchetto, C. Carromeu, A. Acab, D. Yu, G. Yeo, Y. Mu, G. Chen, F. H. Gage, A. R. Muotri, A model for neural development and treatment of Rett Syndrome using human induced pluripotent stem cells. *Cell*. **143**, 527–539 (2010).
59. M. Frega, K. Linda, J. M. Keller, G. Gümüş-Akay, B. Mossink, J.-R. van Rhijn, M. Negwer, T. Klein Gunnewiek, K. Foreman, N. Kompier, C. Schoenmaker, W. van den Akker, I. van der Werf, A. Oudakker, H. Zhou, T. Kleefstra, D. Schubert, H. van Bokhoven, N. Nadif Kasri, Neuronal network dysfunction in a model for Kleefstra syndrome mediated by enhanced NMDAR signaling. *Nat. Commun.* **10**, 4928 (2019).
60. M. Frega, M. Selten, B. Mossink, J. M. Keller, K. Linda, R. Moerschen, J. Qu, P. Koerner, S. Jansen, A. Oudakker, T. Kleefstra, H. van Bokhoven, H. Zhou, D. Schubert, N. Nadif Kasri, Distinct Pathogenic Genes Causing Intellectual Disability and Autism Exhibit a Common Neuronal Network Hyperactivity Phenotype. *Cell Rep.* **30**, 173-186.e6 (2020).
61. B. Mossink, J.-R. van Rhijn, S. Wang, K. Linda, M. R. Vitale, J. E. M. Zöller, E. J. H. van Hugte, J. Bak, A. H. A. Verboven, M. Selten, M. Negwer, B. L. Latour, I. van der Werf, J. M. Keller, T. M. Klein Gunnewiek, C. Schoenmaker, A. Oudakker, A. Anania, S. Jansen, K.-P. Lesch, M. Frega, H. van Bokhoven, D. Schubert, N. Nadif Kasri, Cadherin-13 is a critical regulator of GABAergic modulation in human stem-cell-derived neuronal networks. *Mol. Psychiatry*. **27**, 1–18 (2022).
62. M. Selten, H. van Bokhoven, N. Nadif Kasri, Inhibitory control of the excitatory/inhibitory balance in psychiatric disorders. *F1000Research*. **7**, 23 (2018).
63. H. S. Bateup, C. A. Johnson, C. L. Denefrio, J. L. Saulnier, K. Kornacker, B. L. Sabatini, Excitatory/inhibitory synaptic imbalance leads to hippocampal hyperexcitability in mouse models of tuberous sclerosis. *Neuron*. **78**, 510–522 (2013).
64. H.-T. Chao, H. Y. Zoghbi, C. Rosenmund, MeCP2 Controls Excitatory Synaptic Strength by Regulating Glutamatergic Synapse Number. *Neuron*. **56**, 58–65 (2007).
65. S. R. Gilman, I. Iossifov, D. Levy, M. Ronemus, M. Wigler, D. Vitkup, Rare *De Novo* Variants Associated with Autism Implicate a Large Functional Network of Genes Involved in Formation and Function of Synapses. *Neuron*. **70**, 898–907 (2011).
66. Y. Liu, H. Ding, T. Yan, L. Liu, L. Yu, Y. Huang, F. Li, Y. Zeng, W. Huang, Y. Zhang, A. Yin, A Novel Multi-Exon Deletion of PACS1 in a Three-Generation Pedigree: Supplements to PACS1 Neurodevelopmental Disorder Spectrum. *Front. Genet.* **12**, 690216 (2021).
67. E. Nair-Gill, M. Bonora, X. Zhong, A. Liu, A. Miranda, N. Stewart, S. Ludwig, J. Russell, T. Gallagher, P. Pinton, B. Beutler, Calcium flux control by Pacs1-Wdr37 promotes lymphocyte quiescence and lymphoproliferative diseases. *EMBO J.* **40**, e104888 (2021).
68. A. Butler, P. Hoffman, P. Smibert, E. Papalexi, R. Satija, Integrating single-cell transcriptomic data across different conditions, technologies, and species. *Nat. Biotechnol.* **36**, 411–420 (2018).
69. T. Stuart, A. Butler, P. Hoffman, C. Hafemeister, E. Papalexi, W. M. Mauck, Y. Hao, M. Stoeckius, P. Smibert, R. Satija, Comprehensive Integration of Single-Cell Data. *Cell*. **177**, 1888-1902.e21 (2019).

70. C. S. McGinnis, L. M. Murrow, Z. J. Gartner, DoubletFinder: Doublet Detection in Single-Cell RNA Sequencing Data Using Artificial Nearest Neighbors. *Cell Syst.* **8**, 329-337.e4 (2019).
71. E. A. K. DePasquale, D. J. Schnell, P.-J. Van Camp, Í. Valiente-Alandí, B. C. Blaxall, H. L. Grimes, H. Singh, N. Salomonis, DoubletDecon: Deconvoluting Doublets from Single-Cell RNA-Sequencing Data. *Cell Rep.* **29**, 1718-1727.e8 (2019).
72. R. Fu, A. E. Gillen, R. M. Sheridan, C. Tian, M. Daya, Y. Hao, J. R. Hesselberth, K. A. Riemondy, clustifyr: an R package for automated single-cell RNA sequencing cluster classification. *F1000Research*. **9**, 223 (2020).
73. A. Bhaduri, M. G. Andrews, W. Mancia Leon, D. Jung, D. Shin, D. Allen, D. Jung, G. Schmunk, M. Haeussler, J. Salma, A. A. Pollen, T. J. Nowakowski, A. R. Kriegstein, Cell stress in cortical organoids impairs molecular subtype specification. *Nature*. **578**, 142–148 (2020).
74. A. López-Tobón, C. E. Villa, C. Cheroni, S. Trattaro, N. Caporale, P. Conforti, R. Iennaco, M. Lachgar, M. T. Rigoli, B. Marcó de la Cruz, P. Lo Riso, E. Tenderini, F. Troglio, M. De Simone, I. Liste-Noya, G. Macino, M. Pagani, E. Cattaneo, G. Testa, Human Cortical Organoids Expose a Differential Function of GSK3 on Cortical Neurogenesis. *Stem Cell Rep.* **13**, 847–861 (2019).
75. F. Supek, M. Bošnjak, N. Škunca, T. Šmuc, REVIGO summarizes and visualizes long lists of gene ontology terms. *PloS One*. **6**, e21800 (2011).

Acknowledgments

The authors thank Dr. Gemma Carvill for her continued feedback on the project and the lab of Dr. Peter Penzes, particularly Dr. Euan Parnell and Dr. Marc Forrest, for generously providing protocols and antibodies for synapse experiments.

Funding

PACS1 Syndrome Research Foundation (AGG)
National Institutes of Health grant R01NS123163 (AGG)
NCI CCSG P30 CA060553 (Northwestern University Center for Advanced Microscopy)
National Institutes of Health grant 1S10OD025120 (Northwestern Center for Genetic Medicine)

Author contributions

Conceptualization: LER, AGG
Methodology: LER, AGG, JR (Fig. S1*D,E*)
Investigation: LER, AGG, JR (Fig. S1*D,E*), EGP (Fig. *1B,C*; Fig. S2*B,D-F*)
Visualization: LER, AGG
Supervision: LER, AGG
Writing—original draft: LER
Writing—review & editing: LER, AGG

Competing interests

Authors declare that they have no competing interests.

Data and materials availability

ScRNAseq data will be uploaded to the NCBI Gene Expression Omnibus repository. For differential expression analysis, samples GSM3885398, GSM3885387, ERS4649261, ERS4649262, and ERS4649263 were downloaded from GEO.

All code is available upon request. Code used in this study is a compilation from the following sources. Reads were aligned using the 10X Genomics Cell Ranger pipeline. The output matrix files were initially processed with Seurat version 4 following vignettes produced by the Satija lab found at https://satijalab.org/seurat/. Pseudotime analysis was done with Monocle version 3 following the workflow produced by the Trapnell lab found at https://cole-trapnell-lab.github.io/monocle3/. WGCNA version 1.70-3 was performed by following tutorials produced by the Langfelder and Horvath labs found at https://horvath.genetics.ucla.edu/html/CoexpressionNetwork/Rpackages/WGCNA/.

Figures and Tables

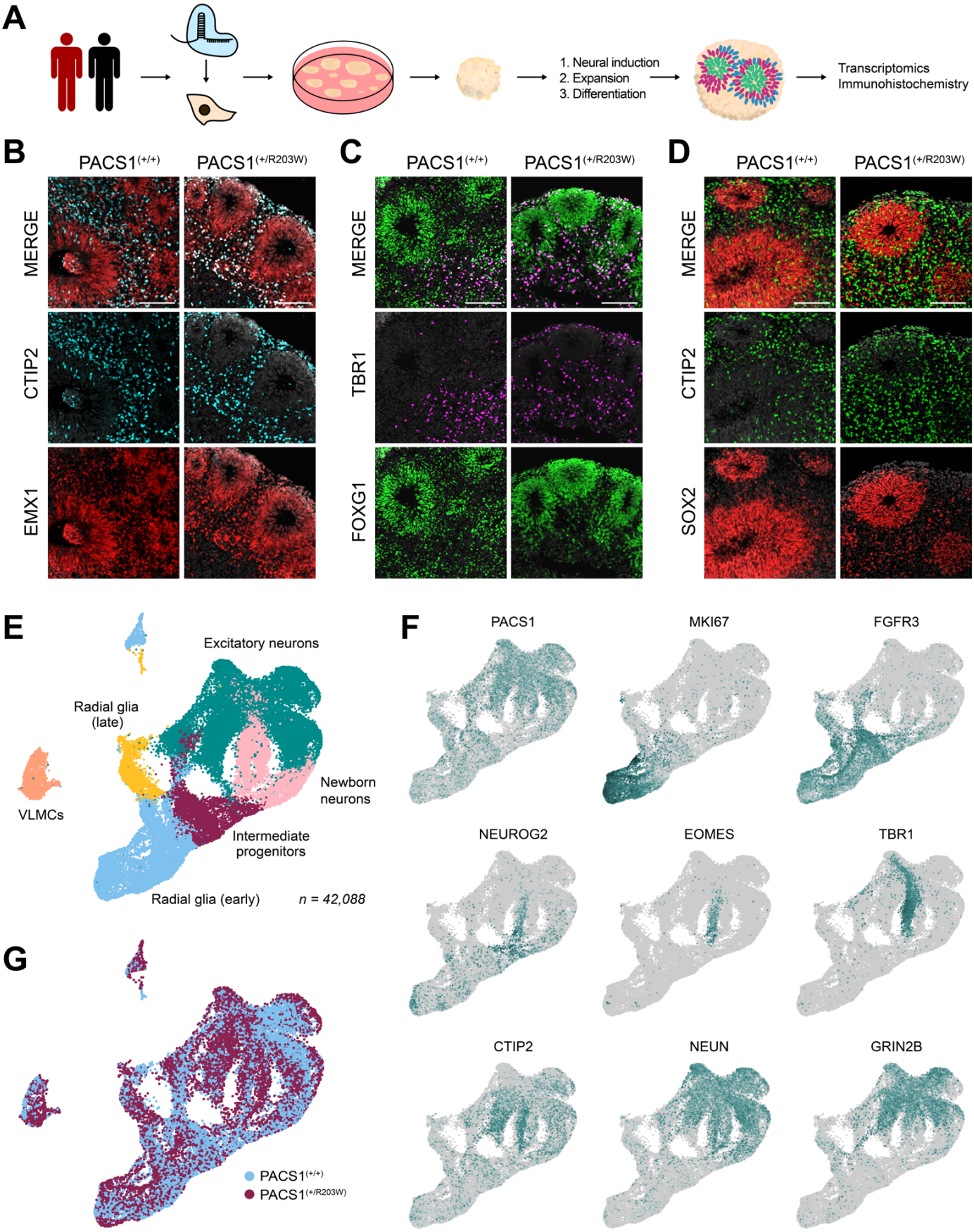

Fig. 1. PACS1 p.R203W variant does not impact cytoarchitectural organization of forebrain organoids. (**A**), Experimental overview. Control, patient, and isogenic cell lines were generated using CRISPR and differentiated to dorsal forebrain organoids through a series of growth factors. Differences between patient and control organoids were then assessed using transcriptomic analysis with immunohistochemistry validation. (**B-D**), Organoids of both genotypes develop SOX2+ ventricular-like zones surrounded by postmitotic TBR1+ and CTIP2+ neurons. Additional dorsal forebrain markers FOXG1 and EMX1 are widely expressed. DAPI is lightly shown in greyscale. Scale bar = 100 µm. (**E**), UMAP dimensionality reduction of all sequenced cells across seven samples. Single-cell RNA sequencing reveals six distinct cell types. (**F**), Feature plots in UMAP space show expression of a transcript in each cell. *PACS1* is expressed in all cell groups, but segregation is observed of proliferative marker *MKI67,* radial glia marker *FGFR3,* intermediate progenitor (IP) marker *NEUROG2*, IP/newborn neuron marker *EOMES*, newborn neuron marker *TBR1,* excitatory projection neuron transcription factor *CTIP2,* pan-neuronal marker *NEUN*, and excitatory synapse subunit *GRIN2B.* (**G**), Distribution of $PACS1^{(+/+)}$ and $PACS1^{(+/R203W)}$ cells in UMAP space. The $PACS1^{(+/R203W)}$ group has been down-sampled to match the number of control cells for visualization purposes.

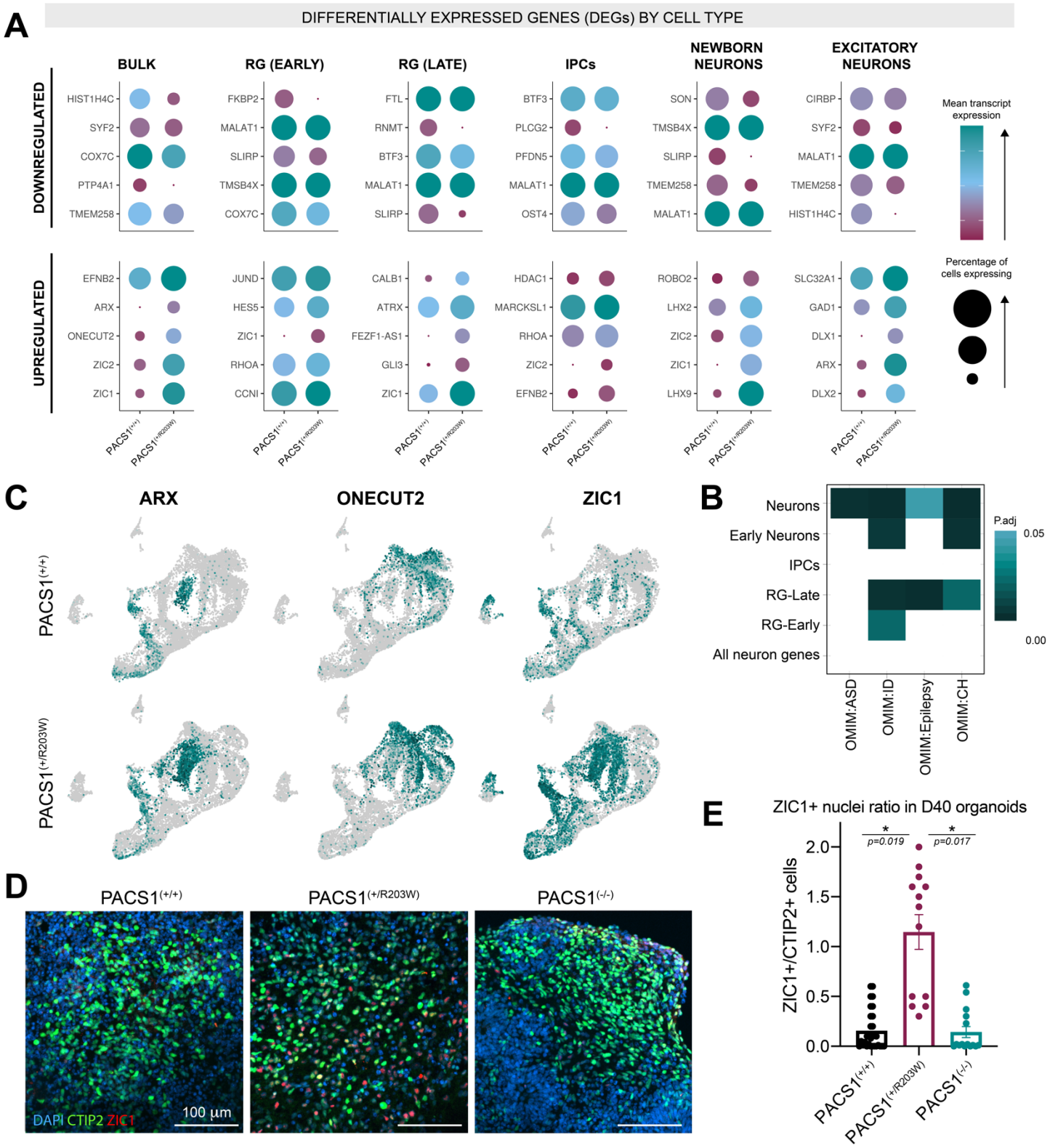

Fig. 2. PACS1 p.R203W variant results in upregulation of risk genes for other neurodevelopmental disorders by a gain-of-function mechanism. (**A**), Top differentially expressed genes (DEGs) between PACS1$^{(+/R203W)}$ and PACS1$^{(+/+)}$ organoids. Ranges of figure legends have been simplified for readability. Complete figure legends for each graph can be found in **Fig. S7***C*. (**B**), *p* values of a gene overlap test between top DEGs in each group and OMIM risk genes for neurodevelopmental disorders with converging phenotypes to PACS1 syndrome, including autism spectrum disorder (ASD), intellectual disability (ID), epilepsy, or cerebellar hypoplasia (CH). *p* values were calculated using a Fisher's exact test with a Benjamini-Hochberg correction for multiple testing. (**C**), Feature plots in UMAP space of top DEGs upregulated in PACS1

syndrome. n=11,851 cells. Expression in each sample – including public controls – can be found in **Fig. S8***A-C.* (**D**), Immunohistochemistry analysis in day 40 organoid sections of CTIP2 and ZIC1 abundance. Scale bar = 100 µm. (**D**), Quantifications of immunohistochemistry analysis in day 40 organoids shown in D, showing mean + SEM. Data is from 28 PACS1$^{(+/+)}$ organoid sections, 13 PACS1$^{(+/R203W)}$ sections, and 16 PACS1$^{(-/-)}$ sections. *p* values are calculated from n = 6 PACS1$^{(+/+)}$ organoids, n = 3 PACS1$^{(+/R203W)}$ organoids, and n = 3 PACS1$^{(-/-)}$ organoids. Values were calculated using a two-tailed t test assuming unequal variance. More detailed descriptions of cell lines and organoids in each calculation can be found in **Fig. S8***D* and **Table S2.**

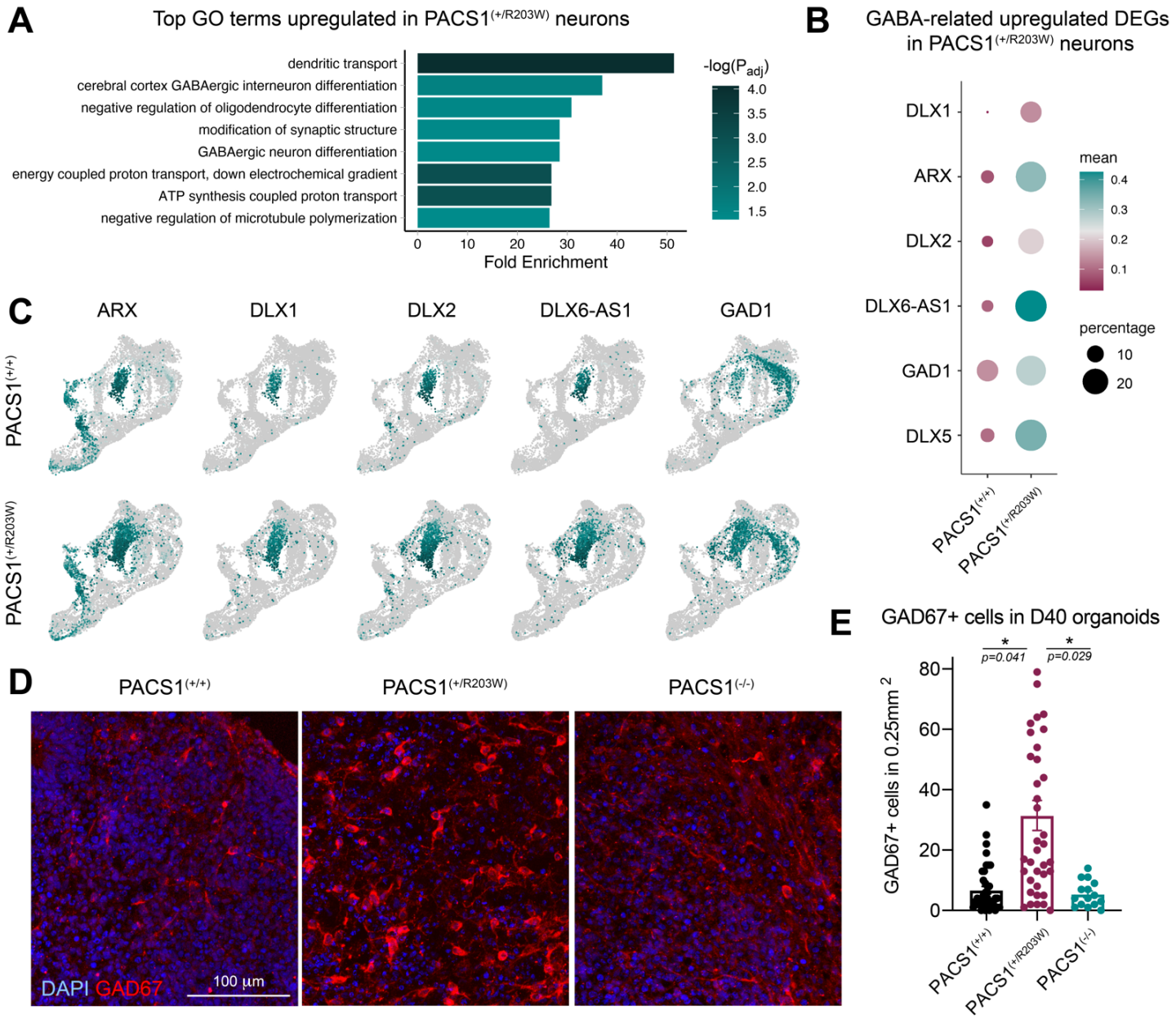

Fig. 3. PACS1$^{(+/R203W)}$ neurons have ectopic GABAergic expression. (**A**), Top GO results for upregulated genes in PACS1$^{(+/R203W)}$ neurons, arranged by fold enrichment. *p* value was calculated using a Fisher's exact test with FDR adjustment. (**B**), Dot plots of differentially expressed genes (DEGs) involved in GABAergic differentiation in PACS1$^{(+/+)}$ vs PACS1$^{(+/R203W)}$ neurons. (**C**), Feature plots in UMAP space of DEGs involved in GABAergic differentiation in PACS1$^{(+/+)}$ and PACS1$^{(+/R203W)}$ neurons. n=11,851. (**D**), Immunohistochemistry analysis of GAD67 expression (the protein product of the gene *GAD1*) in day 40 organoids. Scale bar = 100 µm. (**E**), Quantification of GAD67+ soma per 500x500 micron area in day 40 organoids showing mean + SEM. Data shown is from 40 PACS1$^{(+/+)}$ organoid sections, 46 PACS1$^{(+/R203W)}$ sections, and 15 PACS1$^{(-/-)}$ sections. *p* values are calculated from n = 10 PACS1$^{(+/+)}$ organoids, n = 9 PACS1$^{(+/R203W)}$ organoids, and n = 10 PACS1$^{(-/-)}$ organoids. Values were calculated using a two-tailed t test assuming unequal variance. Detailed descriptions of cell lines and organoids in each calculation can be found in **Fig. S8***E* and **Table S2.**

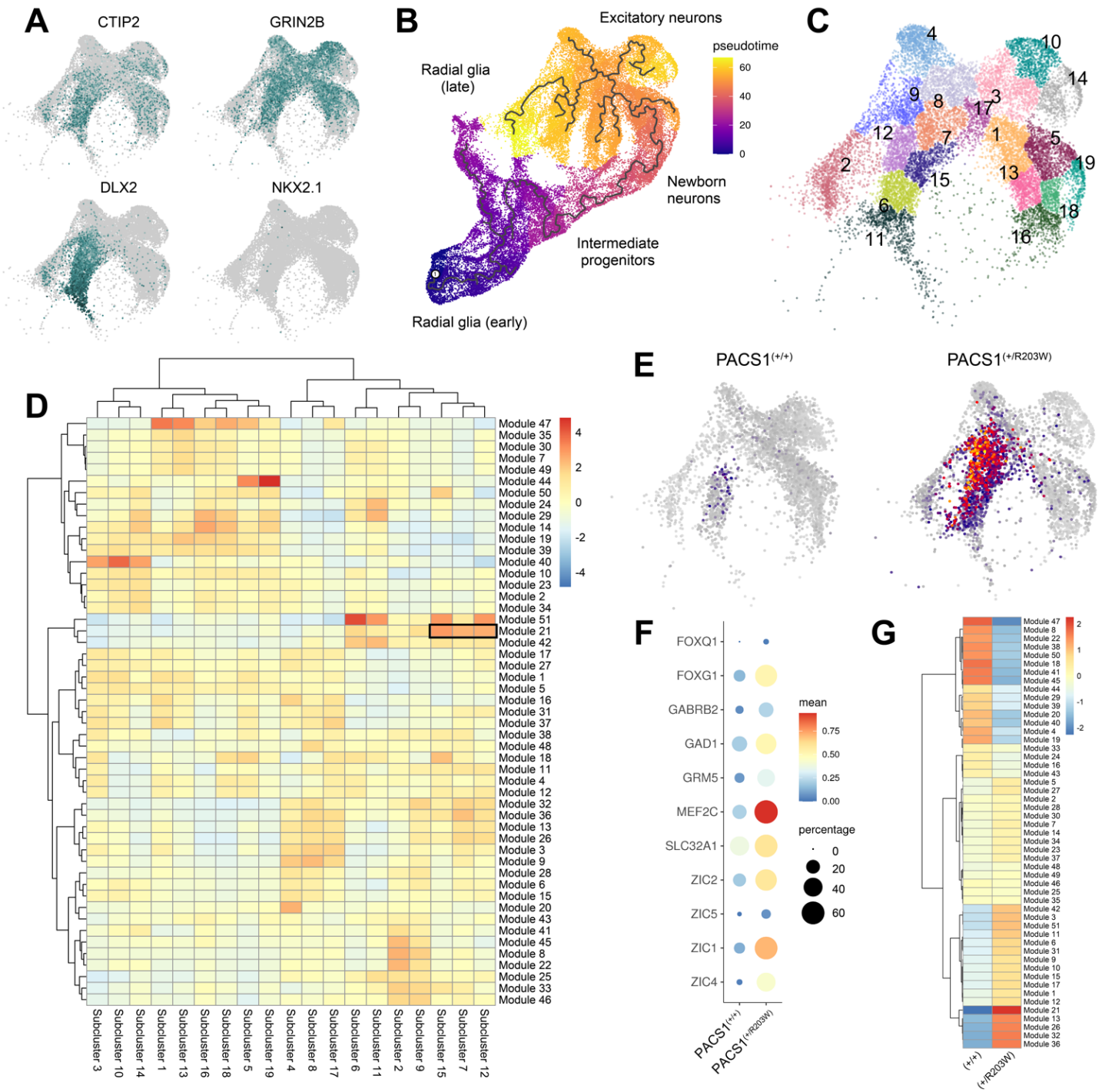

Fig. 4. GABAergic expression is driven by a module including *ZIC* genes. (**A**), Feature plots show a subset of the neuron group demonstrates colocalization of glutamatergic markers such as *CTIP2* and *GRIN2B* with GABAergic marker *DLX2,* as well as an absence of medial ganglionic eminence marker *NKX2.1*. (**B**), A pseudotime trajectory shows progression in pseudoage from radial glia to neurons. (**C**), The neuron group is subclustered at a higher resolution. (**D**), Heatmap of aggregate expression of distinct gene clusters that vary over pseudotime in each subcluster shown in C. Note module 21 is specifically expressed in subclusters 7, 12, and 15, which are just prior to and entering the *DLX2*+ branch. (**E**), Feature plots showing aggregate expression of transcripts in module 21 segregated by genotype. (**F**), Dot plots of select module 21 genes show enhanced expression in PACS1$^{(+/R203W)}$ cells. (**G**), Heatmap of aggregate expression of gene modules in cells just entering the GABAergic branch (clusters 7, 12, and 15 in panel C).

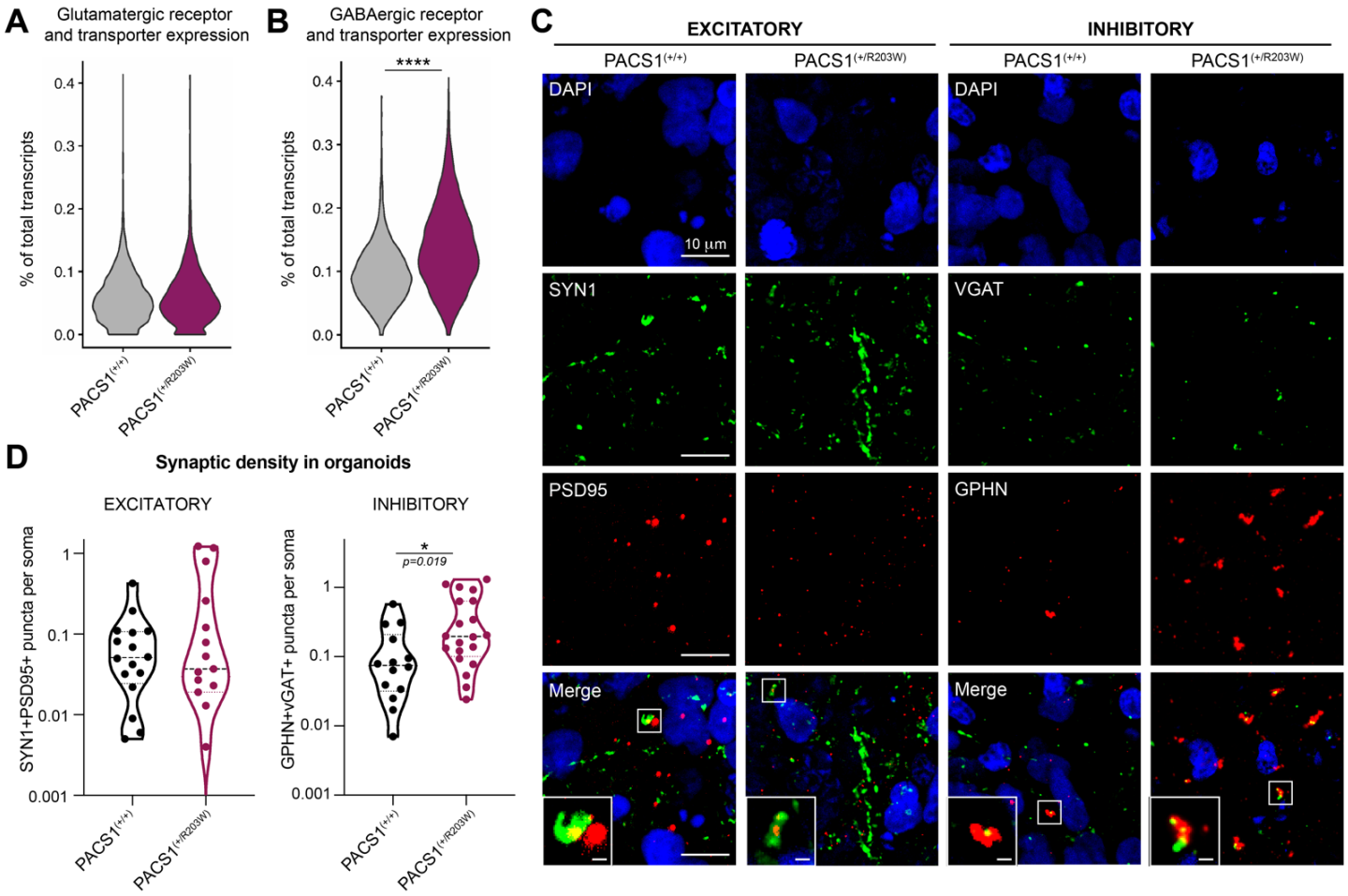

Fig. 5. PACS1$^{(+/R203W)}$ neurons have an increased density of inhibitory synapses. (**A**), Percentage of total transcripts that comprise glutamatergic receptors or transporters. A full list of genes used is in **Fig. S11***A*. $p = 1$ was calculated using a two-sided Wilcoxon rank-sum test with Bonferroni correction for all cells. (**B**), Percentage of total transcripts that comprise GABAergic receptors or transporters. A full list of genes used is in **Fig. S11***A*. p= 8.07e-258 was calculated using a two-sided Wilcoxon rank-sum test with Bonferroni correction for all cells. (**C**), Expression of excitatory and inhibitory synapse markers in day 79 organoid sections. Co-localization of pre-synaptic marker SYN1 and post-synaptic marker PSD95 was used to identify excitatory synapses, while co-localization of post-synaptic marker GPHN and pre-synaptic marker vGAT was used to define inhibitory synapses. Scale bar = 10 µm in the main panels and 1 µm in the zoomed panel. (**D**), Quantification of colocalized synaptic puncta as shown in C. The dashed lines show the median and the dotted lines indicates quartiles. Data is from n=14-20 organoid sections across 4 PACS1$^{(+/+)}$ and 5 PACS1$^{(+/R203W)}$ organoids. $p = 0.15$ for excitatory and 0.019 for inhibitory synapses. Values were calculated using a two-tailed t test assuming unequal variance. Detailed descriptions of cell lines and organoids in each calculation can be found in **Fig. S11***D,E* and **Table S2.**

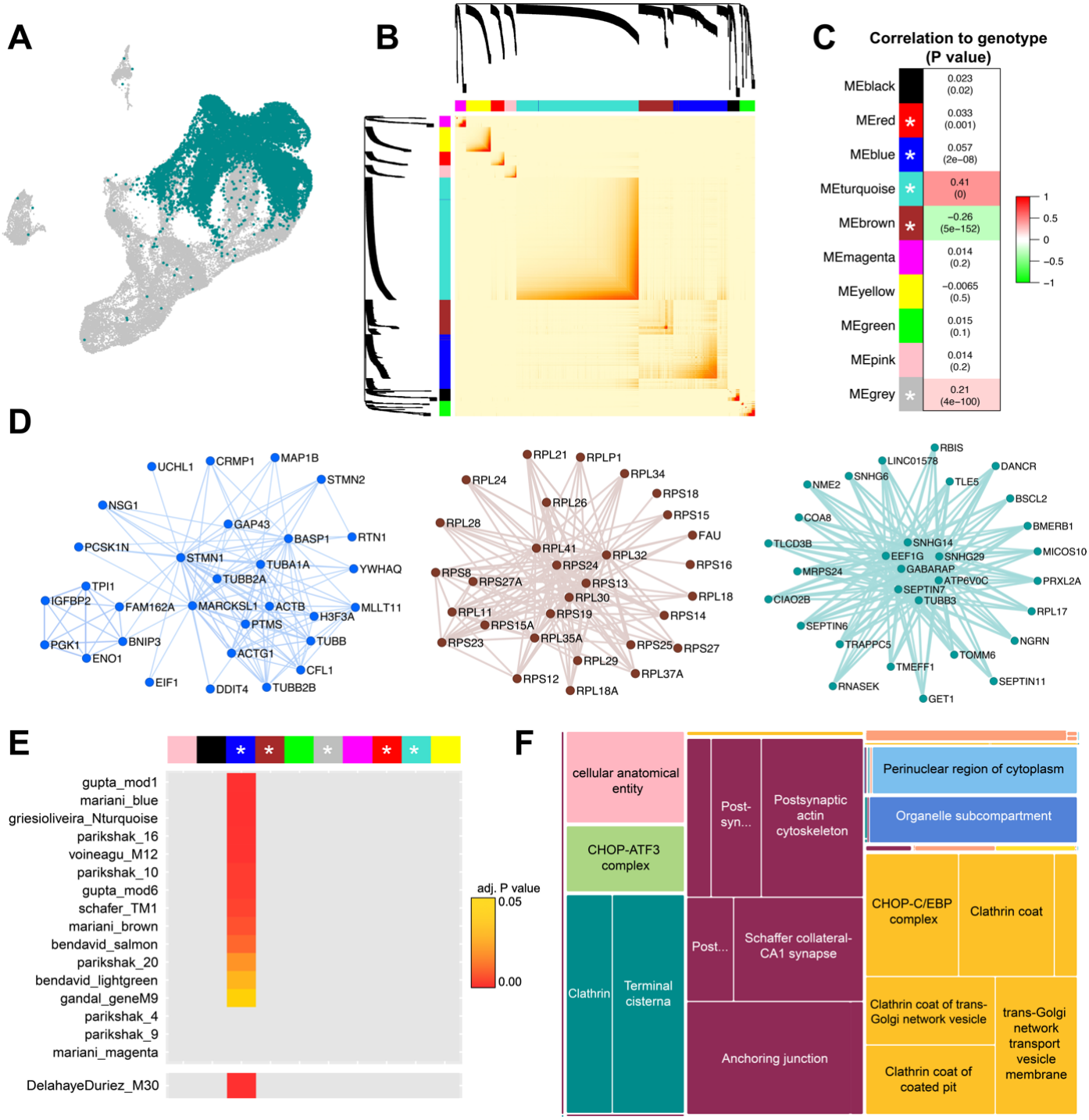

Fig. 6. Gene co-expression analysis reveals an ASD-specific gene network upregulated in PACS1$^{(+/R203W)}$ neurons. (**A**), Input for WGCNA was 4,884 control and PACS1$^{(+/R203W)}$ cells (highlighted). (**B**), A topological overlap matrix shows hierarchical clustering of genes into modules based on their relative interconnectedness. (**C**), 10 distinct gene modules were identified with WGCNA. Correlation was calculated using the Pearson method. *p* value was calculated using a student asymptotic *p* value test. White stars indicate significant correlation to genotype after Bonferroni correction. (**D**), Top 30 gene members of the modules with a positive relationship between a gene's association with genotype and connectedness within a module. Mitochondrial transcripts were removed from the blue module. (**E**), Heatmap showing *p* values from a gene overlap test between module members identified in this study, and neuronal ASD-specific modules from eight other studies and one epilepsy-specific module. *p* values were calculated using Fisher's exact test and corrected using the Benjamini-Hochberg procedure. (**F**), A tree map generated with Revigo (*75*) of GO cellular component analysis of the blue module members. Area size correlates to number of associated GO terms.